Results in Physics 10 (2018) 256–263

Contents lists available at ScienceDirect

Results in Physics

journal homepage: www.elsevier.com/locate/rinp

Flow interference of two side-by-side square cylinders using IB-LBM – Effect of corner radius

Ehsan Adeeb, Basharat Ali Haider, Chang Hyun Sohn*

School of Mechanical Engineering, Kyungpook National University, Daegu 41566, South Korea

ARTICLE INFO

Keywords:
Square cylinder
Circular cylinder
Corner radius
Side by side arrangement
Immersed boundary method
Lattice Boltzmann method
Rounded corners

ABSTRACT

In this study, a two-dimensional Immersed Boundary Lattice Boltzmann Method (IB-LBM) is employed to investigate computationally effect of flow past a pair of square cylinders in side-by-side arrangement at $Re = 100$, for various corner radii. Numerical simulations were performed simultaneously by varying center to center distance between two cylinders (1.5–5.0 D) in the transverse direction and by changing the corner radius (R) from R/D = 0.0 (square) to 0.5 (circular) with 0.1 increment. Aerodynamic characteristics, including the lift and drag coefficients, were quantitatively calculated and compared with each other. Vorticity contours were used as visualization aids to understand the wake pattern and underlying mechanism. The results indicate different features in lift and drag time histories and in wake patterns for a selected range. The numerical results reveal that the flow characteristics and vortex shedding depend significantly on the corner radius and gap spacing. A square cylinder exhibited the maximum average drag value, and the inverse was observed in the case of a circular cylinder. Furthermore, aerodynamic forces were reduced by rounding the corner radius.

Introduction

In recent decades, extensive studies have examined flow over a single cylinder, because it is a significant engineering problem, but the flow over arrays of objects is a practical concern. Objects are repeatedly observed in groups, including chimney stacks, bridge piers, offshore platforms, and chemical reaction towers. In view of controlling vortex shedding, different strategies have been applied by researchers to control fluctuating vortex shedding induced forces on a bluff body to avoid structural failure.

An elaborate method involves controlling the separation point and modifying the shape of the body. However, most flows comprise simple geometrical shapes, although a complex fluid flow or configuration is a challenge in the field of fluid dynamics. In nature, the simplest forms of multiple structures occur in pairs that can be arranged in tandem, side by side, and in staggered configurations. A widespread review of these diverse flow conditions was given by Zdravkovich [1,2] for a circular cylinder at a high Reynolds number. Thus, considerable attention focused on the flow around circular cylinders, and scattered data are available on the square cylinder. However, in nature, abundant engineering structures are available with rectangular, square, and circular cross-section areas.

The flow around a square cylinder was examined experimentally [3,4] and numerically [5–7] by different researchers. The main objective of these studies involved determining the effect of the Strouhal number and drag coefficient on the Reynolds number and on blockage ratio. Tamura et al. [8] experimentally investigated the turbulent flow around different bodies by using a wind tunnel. In turbulent flows, a shear layer aids in reattaching the flow on the side surface of a square cylinder that detaches from the windward edge, even at a 0° angle of attack.

Dalton et al. [9] performed a 2D numerical simulation by using Navier-Stokes equations to simulate the flow around a diamond shaped cylinder and a square cylinder in Reynolds number range of 250–1000. They concluded that instability around the structures is reduced in the laminar and turbulent region by rounding the corners. Miran and Sohn [10] numerically investigated the effect of the rounded corner for a single cylinder by using Navier-Stokes equations for Reynolds number 500. They found that square cylinder had the smallest Strouhal number and increased with the increase of corner radius. Furthermore, they reported minimum values of the mean drag coefficient and root mean square (RMS) values of the lift coefficient at R/D = 0.2.

The flow characteristic around two square cylinders is more complex than that around a single cylinder. Yen and Liu [11] experimentally studied the wake flow of two side-by-side square cylinders by varying the distance ($0 < T/D < 12$) at Reynolds numbers $2262 < Re < 28,000$ where T/D is center-to-center distance between the two cylinders. They classified the flow into the following three regimes:

* Corresponding author.
E-mail addresses: ehsan_adeeb@hotmail.com (E. Adeeb), chsohn@knu.ac.kr (C.H. Sohn).

https://doi.org/10.1016/j.rinp.2018.05.039
Received 11 April 2018; Received in revised form 16 May 2018; Accepted 23 May 2018
Available online 07 June 2018

single mode vortex shedding (T/ D< 0.1), gap flow mode vortex shedding (0.1 < T/ D< 5.5), and coupled vortex shedding mode (T/ D> 5.5).

Kolar et al. [12] experimentally measured the wake feature of two side-by-side square cylinders at a Reynolds number of 23, 100 and found that vortex created from the gap decayed quickly when compared with created from the body. They also observed a predominant vortex street in the anti-phase mode. The main focus of the study was a synchronized regime. Alam and Zohu [13,14] used a flow visualization technique at a low Reynolds number of 300 and reported four regimes based on T/D, as follows: a single body regime for (T/ D< 0.2), wide street regime for 0.2 < T/ D< 1.1, transitional regime for 1.1 < T/ D< 1.4, and coupled regime for all other spacing ratios. Burattimi et al. [15] numerically examined the flow around two square cylinders at a Reynolds number of 73 and reported different ranges of the wake flow regimes, and their results are consistent with those of Agrawal et al. [16], who used a different numerical technique.

With respect to flow around two circular cylinders, many researchers experimentally studied the side-by-side arrangement for the intermediary ratio (1.0 to 3.0), where the wakes interaction occurred strongly for a very high Reynolds number [17–19]. In these studies, they concluded that, at small spacing ratios, the flow wake behind the cylinder is asymmetrical and symmetrical for large spacing ratios. In one experiment by Xu et al. [20], they investigated the gap spacing and Reynolds number effect for a cylinder in a side-by-side configuration using a fluorescence flow visualization technique. They concluded that the Reynolds number can alter the formation of two vortex streets. A technique blending the finite-difference and finite-element methods was applied by Chang and Song [21] to investigate flow features, and it showed different wake flow patterns around two side-by-side cylinders.

As shown by prior researchers, the wake flow pattern is completely dependent on the distance between two cylinders and the Reynolds numbers. However, previous studies mainly focused only on the square and circular cylinders. Therefore, there is a paucity of studies examining a low Reynolds number regime for two square cylinders in a side-by-side arrangement by varying the corner radius, and this should be examined further. Additionally, it is necessary to document and understand variations between the flow properties.

The purpose of this study is to investigate systematically and thoroughly the wake flow of two square cylinders by varying the corner radius to understand the effect of the gap spacing's role and the wake flow pattern at a Reynolds number of 100. For the Fluid Structure Interaction (FSI) problem, complex geometrical shapes normally depend on an unstructured and body-fitted grid. A somewhat unconventional alternative approach is the Immersed Boundary Method (IBM), which has a benefit over conventional approaches for addressing the stationary, moving, and flexible FSI problems. In this study, the Immersed Boundary Lattice Boltzmann Method (IB-LBM) was employed to study the wake pattern and measure the aerodynamic flow quantities.

Computational methodology

Geometrical configuration and boundary condition

The system of interest involves examining the behavior of flow past two side-by-side cylinders for various corner radii in a channel. Fig. 1(a) shows the boundary condition and geometry of the computational domain for IB-LBM analysis. Two equal square cylinders with a dimension of D are separated in the transverse direction (T). The corner radius of a square cylinder, as in Fig. 1(b), is varied as $0.0 \leqslant R/D \leqslant 0.5$, where R denotes the corner radius, and six corner radii are used with an increment of 0.1. The non-dimensional distance (T/D) between two cylinders is varied from 1.5 to 5.0, and a total of six gap ratios (1.5, 2.0, 2.5, 3.0, 4.0, and 5.0) are examined in this numerical study.

The origin of the computing domain is considered at (0, 0). The surface of the cylinder is assumed as no-slip. Top and bottom boundaries of the domain are considered at a transversal distance of 25D from the upper and lower cylinders, respectively, and considered as a free-stream with $U = U_\infty$ and $v = 0$. The formulation of the boundary condition in LBM framework is considered as Guo [22]. A uniform velocity profile is prescribed at the inlet, and it is considered as 20D from the cylinder (L_u). A far field is enacted such that it does not affect the vortices formed in the wake region of the cylinder. An outflow boundary condition (zero normal pressure gradient) is assumed for the outlet with ambient properties and considered at a distance (L_d) of 40D that is sufficiently far to be considered as a far field.

Mathematical formulation

Lattice Boltzmann method

A two-dimensional immersed boundary lattice Boltzmann in-house code was developed to simulate the interaction of fluid flows in the present study. Frisch et al. [23] pioneered the idea of the principle of many particles on the nodes. Collision and propagation are two major steps in this scheme. At each time step, the particles collide with each other and change their velocities, although the net mass and momentum remain the same. In this study, a D2Q9 scheme (D2 represents two dimensions and Q9 refer to the nine particles) is employed with a single relaxation time factor Bhatnagar Gross Krook (BGK) [24,25], which is expressed as follows:

$$f_i(\vec{r} + \vec{c}_i\delta t, t + \delta t) - f_i(\vec{r}, t) = -\frac{\delta t}{\tau}(f_i(\vec{r}, t) - f_i^{eq}(\vec{r}, t)) + \vec{G}_i(\vec{r}, t)\delta t \tag{1}$$

where τ denotes the time to relax the populations toward an equilibrium function f_i^{eq}, $f_i(\vec{r}, t)$ denotes the discrete velocity distribution function, $\vec{c}_i = (c_{ix}, c_{iy})$ denotes velocity at any lattice site $\vec{r} = (x, y)$, $\vec{G}_i$ denotes the external body force, and t denotes time. The equilibrium density function and $\vec{G}_i$ are expressed as follows:

$$f_i^{eq}(\vec{r}, t) = \rho w_i\left[1 + \frac{\vec{c}_i\cdot\vec{u}}{c_s^2} + \frac{(\vec{c}_i\cdot\vec{u})^2}{2c_s^4} - \frac{\vec{u}\cdot\vec{u}}{2c_s^2}\right] \tag{2}$$

$$\vec{G}_i(\vec{r}, t) = \left(1 - \frac{1}{2\tau}\right)w_i\left[\frac{\vec{c}_i - \vec{u}}{c_s^2} + \frac{\vec{c}_i\cdot\vec{u}}{c_s^4}\vec{c}_i\right]\cdot\vec{f} \tag{3}$$

where w_i denote the corresponding weights: $w_0 = 16/36$, $w_i = 4/36$ for $i = 1, 2, 3, 4$, and $w_i = 1/36$ for $i = 5, 6, 7, 8$;ρ denotes the fluid density, f denotes the body force acting on the fluid, $\vec{u} = (u, v)$ denotes the velocity of the fluid at the node, and $c_s = (\delta x/\sqrt{3}t)$ denotes the speed of sound. Velocity vectors for this model are expressed as follows:

$$\vec{c}_i = \begin{cases} (0, 0) & \text{for } i = 0 \\ \left(\cos\left[\frac{\pi(i-1)}{2}\right], \sin\left[\frac{\pi(i-1)}{2}\right]\right)\frac{\delta\vec{r}}{\delta t} & \text{for } i = 1, \ldots, 4 \\ \left(\cos\left[\frac{\pi(2i-9)}{4}\right], \sin\left[\frac{\pi(2i-9)}{4}\right]\right)\sqrt{2}\frac{\delta\vec{r}}{\delta t} & \text{for } i = 5, \ldots, 8 \end{cases} \tag{4}$$

where δt denotes the time step and $\delta\vec{r} = (\delta x, \delta y)$ is the lattice spacing in which fluid particles move to nodes. These equations of collision and propagation are applied iteratively, and the boundary condition is applied after the propagation. The macroscopic fluid velocity $\vec{u}$ and density ρ at a node are expressed as follows:

$$\rho = \sum_i f_i \tag{5}$$

$$\rho\vec{u} = \sum_i \vec{c}_i f_i + \frac{1}{2}\vec{f}\,\delta t \tag{6}$$

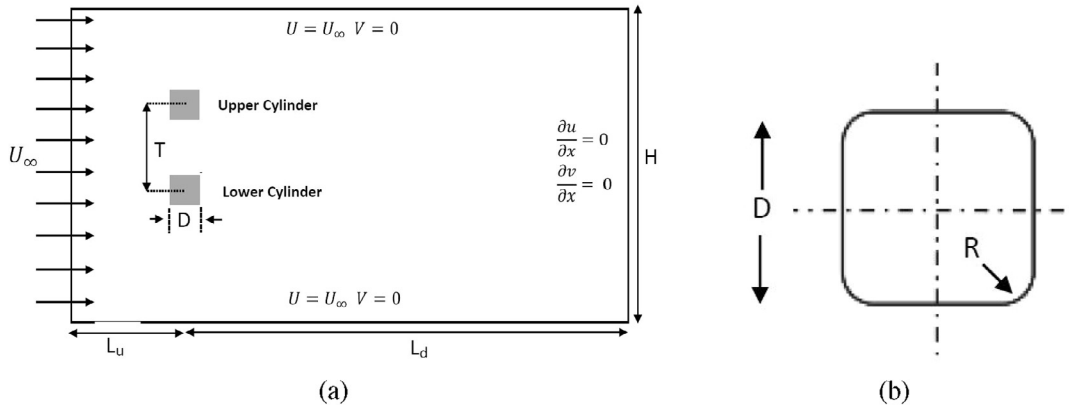

Fig. 1. Geometric configuration (a) computational domain with boundary condition (b) corner radius.

Velocity corrected immersed boundary method

To mimic the no-slip boundary condition, a velocity correction based immersed boundary method (Wang et al. [26]) is coupled with LBM. In the formulation, the velocity is modified in the neighboring points of the immersed boundary. The corrected velocity field is obtained by a Lagrangian interpolation to satisfy the no-slip boundary condition at the boundary intersection points (p_x, p_y) (Fig. 2(a)), as follows:

$$u_k^c = \sum_i \left(\prod_{\mathbf{i} \neq \mathbf{j}} \frac{r_k - r_j}{r_i - r_j} \right) u_i \tag{7}$$

where k denotes the velocity corrected points. a and b at the horizontal mesh line, c and d at the vertical mesh line, i denotes the points in the x-direction (p_x, a, a_1, b, and b_1), and j denotes the points along the y-direction (p_y, c, c_1, d, and d_1). The mean value is used if the velocity is modified more than once at a mesh point. Subsequently, the corrected velocity is used to determine the body force, as follows:

$$\vec{f} = 2\rho \frac{\vec{u}^c - \vec{u}^*}{\delta t} \tag{8}$$

In the study, the non-dimensional form of drag and lift forces is expressed as follows:

$$C_D = \frac{F_D}{0.5\rho U^2 D}; \quad C_L = \frac{F_L}{0.5\rho U^2 D} \tag{9}$$

where C_L and C_D denote the lift and drag force per unit length, respectively. The Root Mean Square (RMS) value of the lift coefficient is expressed as follows:

$$C_{LRMS} = \sqrt{\frac{1}{N} \sum_{j=1}^{N} (C_{L,j})^2} \tag{10}$$

where N defines the number of the time steps, and $C_{L,j}$ defines the instantaneous lift coefficient. To obtain accurate results, the time averaged value of drag and lift is computed after the solution achieves steady state periodicity. The Strouhal number is defined as, where F is vortex shedding frequency:

$$St = \frac{FD}{U} \tag{11}$$

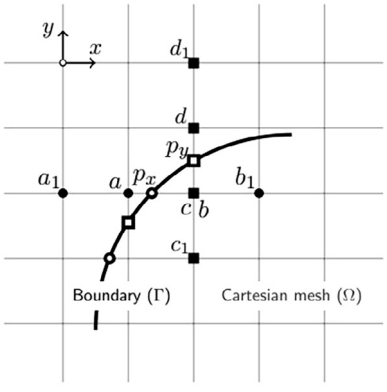

Fig. 2. Immersed-boundary [26] intersection points (hollow circles) with a horizontal grid line; boundary intersection points (hollow square) with a vertical grid line; and boundary-dependent points (solid circles) along the horizontal grid line.

Grid independence study

In this study, three cases of mesh size are employed, namely, G1, G2, and G3, for the mesh independent study. The remaining parameters for the mesh generation and a comparison between the meshes is given in Table 1 for flow past a square and circular cylinder.

In addition to a comparison of grid dependence, aerodynamics quantities are acquired and equated with previous data, and these are listed in Table 2. The results are consistent with those in previous studies, and this ensures the reliability of the code. With respect to the subsequent analysis, all computations are performed by using the G2 grid.

Results and discussion

Wake pattern

Different types of flow pattern occur that totally depend on the transverse spacing between the cylinders. Fig. 3(a) shows the effect of wake pattern around two cylinders in side-by-side configuration at $T/D = 1.5$ by changing corner radius $0.0 \leqslant R/D \leqslant 0.5$. In the downstream, both bodies vortex shedding resembles a single cylinder vortex pattern at each time instance, with a single vortex in the downstream.

Table 1
Grid dependence study.

Grid name	δx	$\overline{C_D}$	St. No.	Type of body
G1	0.050D	1.51	0.148	Square
		1.41	0.158	Circular
G2	0.025D	1.50	0.146	Square
		1.40	0.168	Circular
G3	0.010D	1.50	0.146	Square
		1.40	0.168	Circular

Table 2
Comparison with extant studies at Re 100.

Previous studies	$C_{L,RMS}$	$\overline{C_D}$	St. No.	Type of body
Berrone et al. [27]	–	1.48	0.145	Square
Lam et al. [28]	0.18	1.49	0.144	Square
Present result	0.18	1.50	0.146	Square
Williamson (Exp) [29]	–	–	0.164	Circular
Zdravkovich	–	1.40	0.167	Circular
Kang (Exp) [30]	0.32	1.33	0.165	Circular
Lee and Yang [31]	0.33	1.34	0.165	Circular
Present result	0.33	1.40	0.168	Circular

Inner vortices of upper and lower cylinders interact more intensely and cancel each other's effect. Mainly, vortex shedding occurs only by the outer vortices of both bodies.

At transverse spacing of 2.0D, single vortex patterns become disturbed: one cylinder wake influences another body's wake. Strong interaction of the wakes is observed between bodies when the center-to-center distance is up to 2.0*D* for all corner radii. The instantaneous vorticity contour at 3.0D are shown in Fig. 3(b) which shows a biased wake flow pattern, in addition to an extremely wider wake. The bodies vortex shedding influences each other. Vortices of the same strength are shed exactly at the same time and generate in the form of long strips, as opposed to a round shape for all corner radii. One interesting observation is that a single vortex is shed behind each cylinder and shows a bias: The wake behind one cylinder is larger and wider than that of the other one. This is occasionally observed for the upper cylinder and for the lower cylinder. This biased wake pattern behavior is observed for corner radius $0.0 \leqslant R/D \leqslant 0.4$ until 3.0D, and it is 2.5D for $0.4 < R/D \leqslant 0.5$.

When T/D increases further from the above described corner radius transverse spacing, the interaction between cylinder vortices becomes successively weaker, and vortices shed more independently. It is observed that a vortex from both cylinders never cross the imaginary centerline of the domain. The vortices of the opposite strength from the upper and lower bluff bodies are synchronous and shed collectively. Single-body vortex pattern appear separately for each body and exhibit extremely weak interaction. Separate vortices shed from both the cylinders create a binary vortex street of the wake in the downstream. In terms of the shape of the vortex, they are similar to single bluff body vortices for their respective corner radii. An additional observation is that the wake width is altered by changing the corner radius of the body. A square cylinder ($R/D = 0.0$) results in a wider wake that decreases when the corner radius increases, and the circular cylinder ($R/D = 0.5$) results in the narrow wake (Fig. 3(c)).

Fig. 4 shows the instantaneous vortex pattern when center to center distance is 1.5D for $R/D = 0.0$. At this distance, different kind of vortex pattern is observed for all the corner radii. Fig. 4(a) shows that vortex shedding occurs only because of the free stream sides (outer) of both cylinders. In Fig. 4(b), the upper cylinder free stream side vortex (outer) and lower cylinder inner vortex merge together and shed combined, whereas the inner vortex of the upper cylinder is trapped between them. Fig. 4(c) and (d) show that one of the outer wakes is much longer than normal. Because of the very small gap, the vortex shedding of the wake becomes quite complex, irregular, and arbitrary at this distance. In all the time steps, the inner vortices of both bodies have much less contribution in vortex shedding. Thus, vortex-shedding process occurs arbitrarily, which is observed for all corner radii at this distance. An analysis of the flow pattern until a 2.0D distance indicates that the phenomena of merging vortices is non-periodic, but the shedding pattern remains like that of a single cylinder until 1.5D.

Aerodynamic forces

Lift and drag time histories show different features in a side-by-side configuration by changing the center-to-center distance (T/D) between bodies. However, it shows an in-phase phenomenon for time histories in tandem configuration [1,2] for a circular cylinder. Different features of drag and lift ($R/D = 0.5$) time histories are shown in Fig. 5 with respect to different transverse spacing ratios $T/D = 1.5$, 2.5, and 5.0.

Fig. 5(a) and (b) shows C_L and C_D time histories for a close center-to-

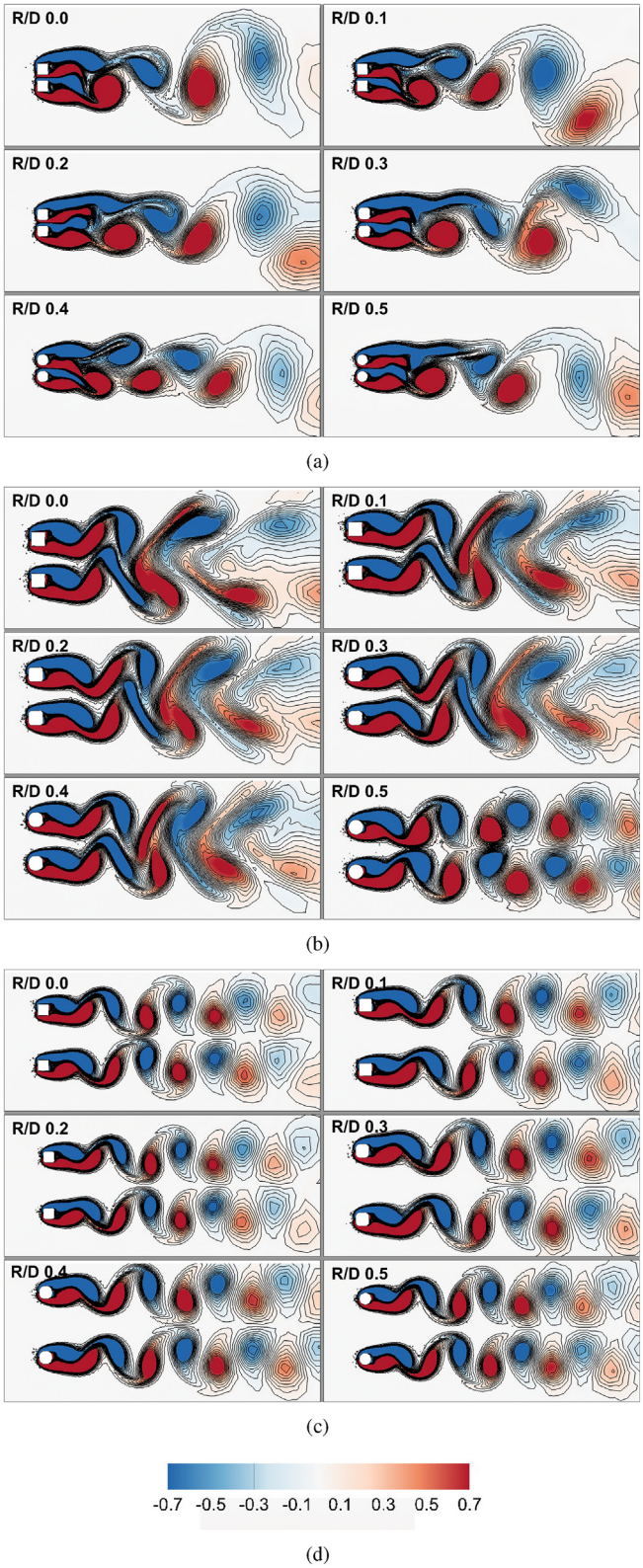

Fig. 3. Wake pattern for all corner radii: T/D (a) 1.5 (b) 3.0 (c) 5.0.

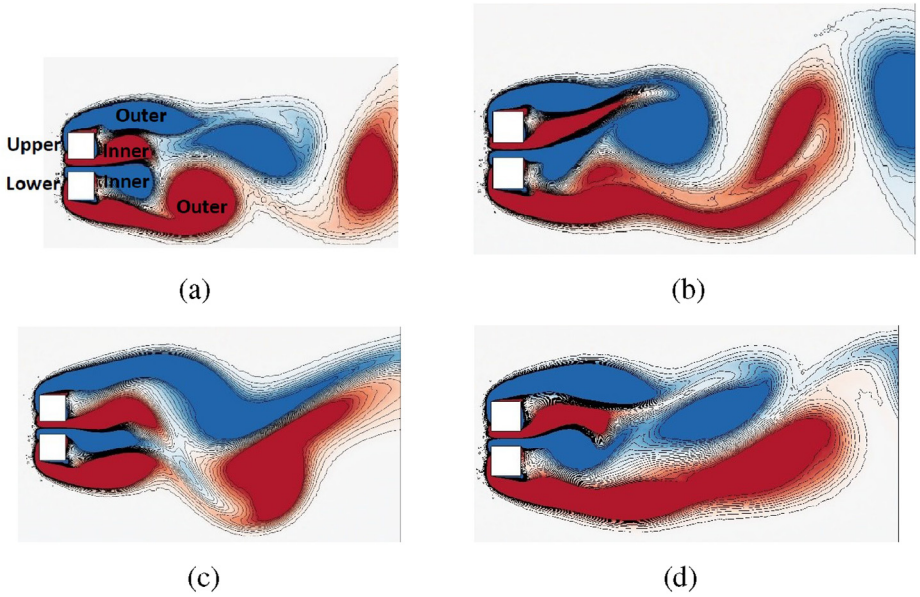

Fig. 4. Instantaneous vortex pattern at T/D = 1.5 for R/D = 0.0: (a) vortex shedding from freestream side (b) inner vortex of upper cylinder trap in between two vortices (c) upper cylinder outer vortex stretched (d) lower cylinder outer vortex stretched.

center distance between bodies (T/ D= 1.5). Time histories show that stabilization never occurs for a periodic pattern and fluctuations occur in time histories, thereby producing non-periodicity in the flow. In a side-by-side arrangement, the overall drag increases on both bodies, in contrast to the tandem arrangement [1,2], in which single-body wake phenomena reduce the drag on the downstream body. The amplitude fluctuation values are low for lift time histories. Both drag and lift exhibit non-periodic behavior, which is observed for a long period compared with other transverse spacing ratios. Similar phenomena are observed for all corner radii ($0.0 \leqslant R/D \leqslant 0.5$) until a 2.0D transverse spacing.

When center to center distance is increased, the shedding pattern changes from periodically unstable and moves towards periodically stable shedding. In this gap ratio (for corner radius $0.0 \leqslant R/D \leqslant 0.4$ till 3D, and it is 2.5D for $0.4 < R/D \leqslant 0.5$) both bodies lift time history shows no-phase difference when flow field get periodic. The reverse is observed in the drag graph as flow get periodically stable drag time histories start showing out of phase phenomena (Fig. 5(b) and (d)). A similar trend is observed for all corner radii. With respect to a side by side arrangement, a different value is observed for R/ D= 0.5 due to corner radius because it is difficult for wakes to interact with each other.

When center-to-center distance further increases (for corner radius $0.0 \leqslant R/D \leqslant 0.4$ greater than 3D, and it is greater than 2.5D for $0.4 < R/D \leqslant 0.5$), the flow in the downstream region stabilizes quickly, and both bodies vortex shedding do not affect each other, as shown in Fig. 5(e) and (f). As the flow in the downstream becomes periodically stable, a phase difference is exhibited by the upper and lower bluff bodies in the lift time history, and no phase difference is observed in the drag graph. The reverse is observed when the transverse spacing is greater than 2.0D. An interesting observation for all the spacing is that the lift coefficients of both bodies exhibit different force amplitudes, where the square cylinder (R/ D= 0.0) exhibits a lower fluctuation when compared with that of a circular cylinder (R/ D= 0.5), and it increases as R/D increases. Overall, a mean negative lift is generated by the upper body, and a mean positive lift is generated by the lower body in all transverse spacing ratios. A transverse gap (T/D = 1.5 and 2.0) between the cylinders (with a lower pressure in the gap and a higher pressure on the sides of the body) forces the flow to pass with increased speed from the gap. Although the mean lift is zero for a single cylindrical object, the pressure difference generated by this transverse arrangement produces a mean negative and positive lift on the bodies.

The effects of the corner radius and transverse spacing on the average drag coefficient are shown in Fig. 6(a) and (b) for the upper and lower bodies, respectively. Drag for the upper and lower bluff bodies exhibit almost identical values, even at a very small distance (T/ D = 1.5), when compared with a tandem arrangement [1–2] in which large variations in aerodynamic coefficients occur when the cylinder is placed in a low spacing ratio. Fig. 6(a) and (b) shows that, by increasing the transverse distance, the drag exhibits a linearly decreasing trend for the upper and lower bodies for all corner radii, and the values approach to their respective corner radii. This is most likely because the gap flow interaction of the bodies becomes insignificantly effective. Additionally, by changing the corner radius, the flow separation is delayed, and this results in less drag on the bluff body. R/D = 0.0 exhibits a maximum value, and R/D = 0.5 exhibits a minimum value.

The mean lift coefficients for the upper and lower cylinders also exhibit identical magnitudes, although with opposite signs; thus, the resultant net lift force is not zero for each cylinder. The effects of the corner radius and gap on C_{LRMS} for the upper and lower bodies are shown in Fig. 7(a) and (b). When center-to-center distance is low (T/ D = 1.5D), R/D = 0.5 exhibits a maximum value, and R/D = 0.0 exhibits a minimum value for C_{LRMS}. Overall, with an increase in the T/D and decrease in R/D (starting from the circular cylinder), the lift trend decreases. As shown in Fig. 7(a) and (b), the interaction for R/D = 0.5 becomes weak earlier compared with the other corner radius bodies, thereby ensuring the absence of interaction with other bluff body wakes. All bodies corner radii exhibit a decreasing trend as transverse spacing increases.

Fig. 8(a) and (b) shows the time-averaged streamlines for R/D = 0.0 and 0.5 at transverse spacing of 2.5D and 4D. At a low gap ratio, both bodies time-averaged streamlines illustrate that they interact with each other strongly. As the transverse spacing value increases, streamlines become independent and do not have any influence on each other.

When both bodies exhibit a close gap, significant changes occur in the flow characteristics, and the wake structure is completely different from that of a single body. An increase in the center-to-center distance between the two bodies makes the interaction weaker, and the gap turns out to be insignificant irrespective of the corner radius. Therefore, the values ultimately approach the single-body corner radius. In the side-by-side configuration, the drag is reduced on both bodies because of the rounding of the corners of a square cylinder and by increasing the

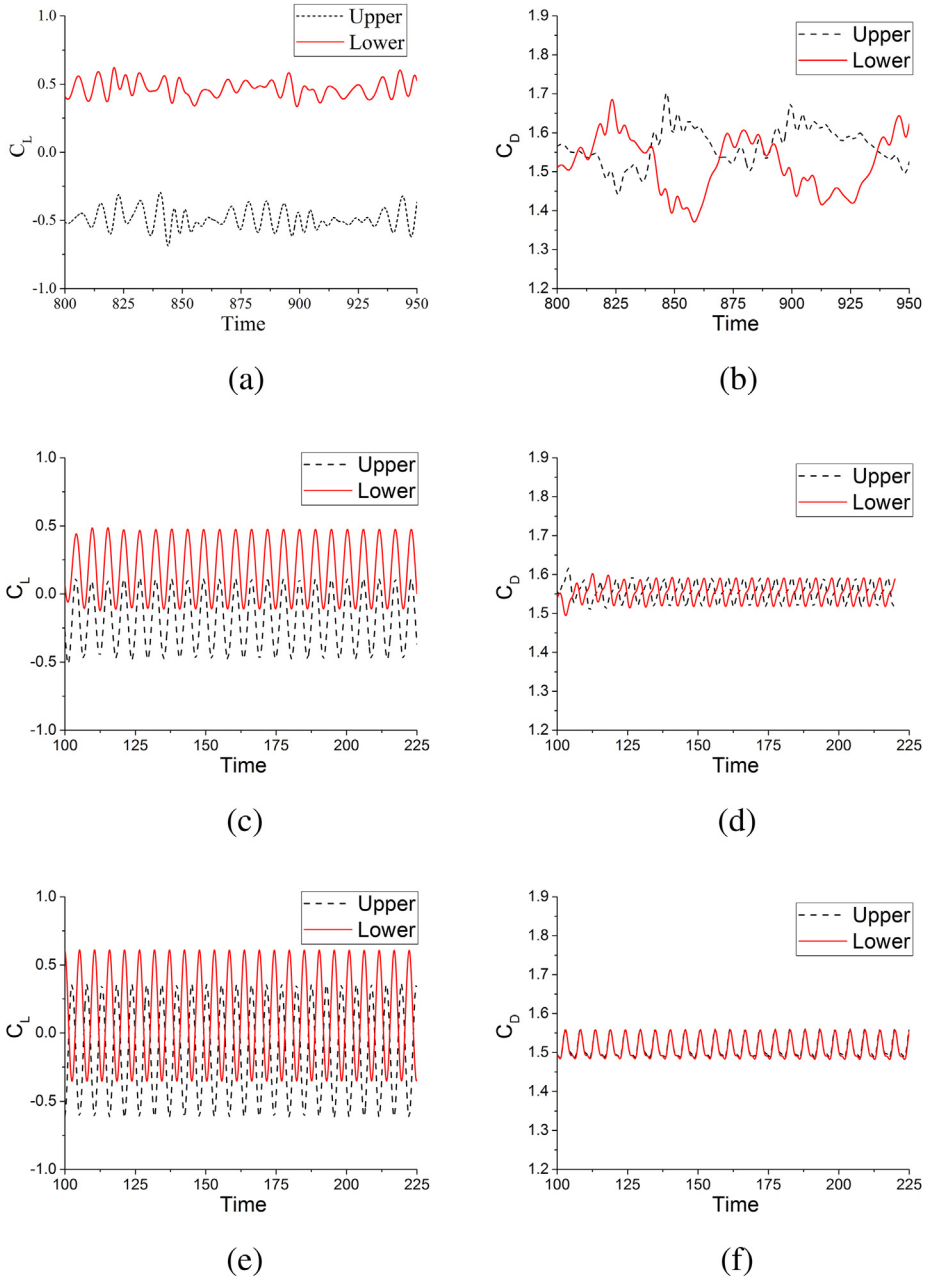

Fig. 5. Time histories of the lift and drag coefficients for R/D = 0.5: (a) T/D = 1.5 (b) T/D = 2.5 (c) T/D = 3.0.

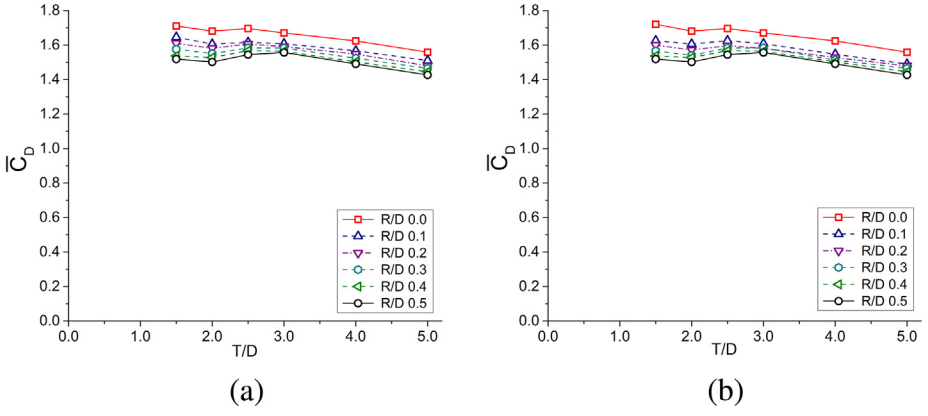

Fig. 6. Variation in the average drag coefficient by varying the corner radius and center-to-center distance: (a) upper cylinder (b) lower cylinder.

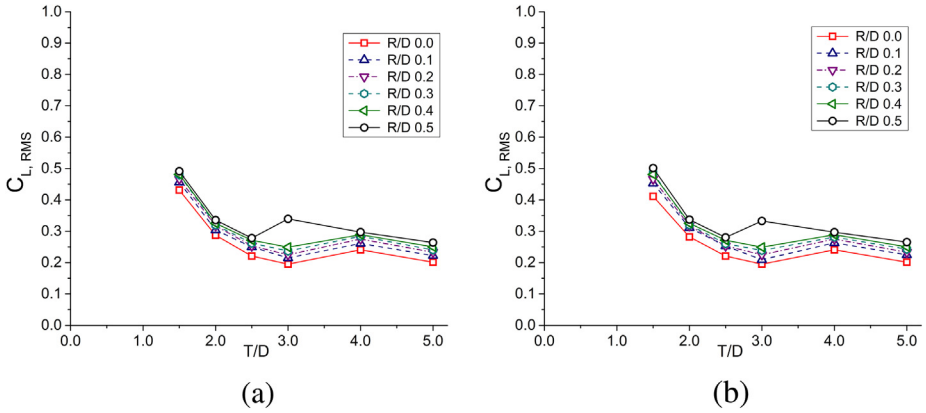

Fig. 7. Variation in RMS lift value by varying corner radius and center-to-center distance: (a) upper cylinder (b) lower cylinder.

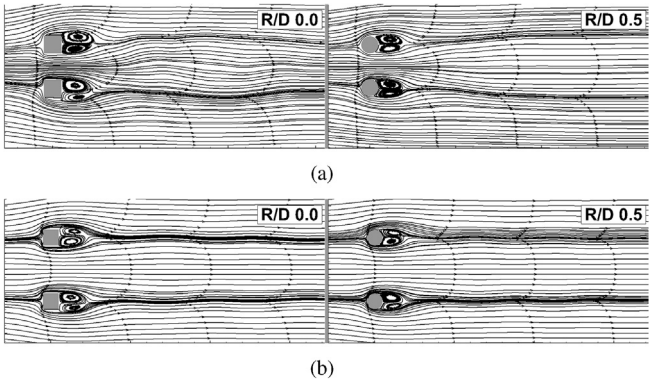

Fig. 8. Averaged streamlines, (a) T/D = 2.5 and (b) T/D = 4.0, for R/D = 0.0 and R/D = 0.5.

T/D.

Conclusions

In this study, the IB-LBM method was used to predict the aerodynamic flow characteristics of a square cylinder in a side-by-side configuration, with different rounded corners at Reynolds number 100. For this purpose, an in-house numerical code was developed and validated with available published data, which shows good agreement with the previous results. In the side-by-side configuration, the drag decreased by rounding the corners of a square cylinder and by increasing the transverse distance.

For $0.0 \leqslant R/D \leqslant 0.5$, $T/D \leqslant 1.5$, both body wakes merged with each other and acted like a single structure wake for all corner radii and shed like a single body. The gap between the two bodies was small and generated a pressure difference that produced mean negative and positive lift for upper and lower bodies, respectively. Thus, R/D = 0.0 (square cylinder) resulted in a larger and wider wake when compared with R/D = 0.5 (circular cylinder) and other corner radius bodies. The flow separation was delayed by changing the corner radius; thus, R/D = 0.0 showed a higher drag value. The time histories for lift and drag never became periodically stable at transverse spacing (1.5D and 2.0D).

For $0.0 \leqslant R/D \leqslant 0.4$ $(2.0 \geqslant T/D \leqslant 3.0)$ and R/D = 0.5 $(2.0 \geqslant T/D \leqslant 2.5)$, the time history (lift and drag) and shedding pattern of flow moved from periodically unstable to periodically stable behavior. Wake bias was observed behind each cylinder, which is completely arbitrary. Thus, there was an impact on each other's wake, which made a much wider wake.

With respect to $0.0 \leqslant R/D \leqslant 0.4$ $(T/D > 3.0)$ and for R/D = 0.5 $(T/D > 2.5)$, the wake interaction between the two cylinders became progressively weaker by increasing the spacing. The wake vortices of both bodies never crossed the imaginary centerline of the domain and produced a single body wake pattern for their respective corner radii. Further, the values of the aerodynamic coefficients approached those of a single body.

Acknowledgment

This work is supported by Basic Science Research Program through the National Research Foundation of Korea (NRF) funded by the Ministry of Education (NRF-2017R1D1A1B03032472).

References

[1] Zdravkovich MM. Review of flow interference between two circular cylinders in various arrangements. J Fluids Eng 1977:618–33.
[2] Zdravkovich MM. The effects of interference between circular cylinders in cross flow. J Fluids Struct 1987:239–61.
[3] Okamoto S, Uemura N. Effect of rounding side corners on aerodynamic forces and turbulent wake of a cube placed on a ground plane. Exp Fluids 1991:58–64.
[4] Saha AK, Muralidhar K, Biswas G. Vortex structures and kinetic energy budget in two-dimensional flow past a square cylinder. Comput Fluids 2000:669–94.
[5] Breuer M, Bernsdorf J, Zeiser T, Durst F. Accurate computations of the laminar flow past a square cylinder based on two different methods: lattice-Boltzmann and finite-volume. Int J Heat Fluid Flow 2000:186–96.
[6] Suzuki H, Inoue Y, Nishimura T, Fukutani F, Suzuki K. Unsteady flow in a channel obstructed by a square rod (crisscross motion of vortex). Int J Heat Fluid Flow 1993:2–9.
[7] Saha AK, Muralidhar K, Biswas G. Experimental study of flow past a square cylinder at high Reynolds numbers. Exp Fluids 2000:553–63.
[8] Tamura T, Miyagi T. The effect of turbulence on aerodynamic forces on a square cylinder with various corner shapes. J Wind Eng Ind Aerodyn 1999:135–45.
[9] Dalton C, Zheng W. Numerical solutions of a viscous uniform approach flow past square and diamond cylinders. J Fluids Struct 2003:455–65.
[10] Miran S, Sohn CH. Numerical study of the rounded corners effect on flow past a square cylinder. Int J Numer Methods Heat Fluid Flow 2015:686–702.
[11] Yen SC, Liu JH. Wake flow behind two side-by-side square cylinders. Int J Heat Fluid Flow 2011:41–51.
[12] Kolar V, Lyn DA, Rodi W. Ensemble averaged measurements in the turbulent near wake of two side-by-side square cylinders. J Fluid Mech 1997:201–37.
[13] Alam MM, Zhou Y, Wang XW. The wake of two side-by-side square cylinders. J Fluid Mech 2011:432–71.
[14] Alam MM, Zhou Y. Intrinsic features of flow around two side-by-side square cylinders. Phys Fluids 2013.
[15] Burattini P, Agrawal A. Wake interaction between two side-by-side square cylinders in channel flow. Comput Fluids 2013:134–42.
[16] Agrawal A, Djenidi L, Antonia RA. Investigation of flow around a pair of side-by-side square cylinders using the lattice Boltzmann method. Comput Fluids 2006:1093–107.
[17] Akilli H, Akar A, Karakus C. Flow characteristics of circular cylinders arranged side-by-side in shallow water. Flow Measure Instrum 2004:187–97.
[18] Eastop TD, Turner JR. Air flow around three cylinders at various pitch to diameter ratios for both a longitudinal and a transverse arrangement. Trans Inst Chem Eng 1982.
[19] Sumners D, Wong SST, Price SJ, Paigdoussis MP. Fluid behaviour of side-by-side circular cylinders in steady cross-flow. J Fluids Struct 1999:309–38.
[20] Xu SJ, Zhou Y, So RMC. Reynolds number effects on the flow structure behind two side-by-side cylinders. Phys Fluids 2003.
[21] Chang KS, Song CJ. Interactive vortex shedding from a pair of circular cylinders in a transverse arrangement. Int J Numer Methods Fluids 1990:317–29.

[22] Guo Z, Zheng C, Shi B. Non-equilibrium extrapolation method for velocity and pressure boundary conditions in the lattice Boltzmann method. Chin Phys 2002:366–74.
[23] Frisch U, Hasslacher B, Pomeau Y. Lattice gas automata for the Navier-Stokes equations. Phys Rev Lett 1986.
[24] Guo Z, Zheng C, Shi B. Discrete lattice effects on the forcing term in the lattice Boltzmann method. Phys Rev E 2002.
[25] Qian YH, Humieres D, Lallemand P. Lattice BGK models for Navier Stokes equation. Europhys Lett 1992:479–84.
[26] Wang X, Shu C, Wu J, Yang LM. A boundary condition implemented immersed boundary lattice Boltzmann method and its application for simulation of flows around a circular cylinder. Adv Appl Math Mech 2014:811–29.
[27] Berrone S, Garbero V, Marro M. Numerical simulation of low Reynolds number flows past rectangular cylinders based on adaptive finite element and finite volume methods. Comput Fluids 2011:92–112.
[28] Lam K, Lin YF, Zou L, Liu Y. Numerical study of flow patterns and force characteristics for square and rectangular cylinders with wavy surfaces. J Fluids Struct 2012:359–77.
[29] Williamson CHK. 2-D and 3-D aspects of the wake of a cylinder and their relation to wake computations. Vortex Dyn Vortex Methods 1991:719–51.
[30] Kang S. Characteristics of flow over two circular cylinders in a side-by-side arrangement at low Reynolds numbers. Phys Fluids 2003:2486–98.
[31] Lee K, Yang KS. Flow patterns past two circular cylinders in proximity. Comput Fluids 2009:778–88.